

Dynamic behavior of a clamped-clamped bi-stable laminate for energy harvesting

Ajay V. Kumar, Myungwon Hwang, Andres F. Arrieta

College of Engineering, School of Mechanical Engineering, Purdue University, 610 Purdue Mall,
West Lafayette, IN USA 47907

ABSTRACT

Multi-stable laminates have many applications in morphing structures, energy harvesting devices, and metamaterials due to the specific characteristics attributed to the exhibited stable states. Changes between stable states allow for large deflections, on-demand variation of the stiffness of compliant structures embedded within these elements, and control of effective dynamic properties in periodic lattices. These changes in state can be accessed via a snap-through instability triggered by introducing a well-defined activation energy. The resulting oscillations could enable broadband energy harvesting via piezoelectric transduction and resistive circuits. In this paper, a clamped-clamped bi-stable laminate is studied to understand the behavior of the laminate at each stable state and determine energy harvesting capabilities. An FEA model is created to determine the frequency and shapes of resonant modes. Certain modal shapes have significant deformations near the clamp which are necessary for piezoelectric elements to generate a voltage. Small amplitude low frequency vibrations are used to excite the laminate at each stable state using a shaker. The laminate is then excited so that inter-well oscillations become present. The resonant characteristics of each stable state determined by the simulations are similar to the experimentally observed responses with some variation. The laminate shows inter-well dynamics at particular resonant frequencies and for a range of frequencies in which both stable states have similar modal characteristics. At higher excitations and a range of frequencies is observed causing chaotic and inter-well oscillations. This shows that the laminate exhibits vibrational dynamics which are capable of enabling broadband energy harvesting devices.

Keywords: Energy, Harvesting, Bi-stable, Metamaterials, Vibrations, Nonlinear

1. INTRODUCTION

Energy harvesting has been studied extensively due to its potential applications in numerous fields^{5, 14, 15, 16, 17}. The ability to gather energy from natural vibrations allows certain devices to be powered wirelessly and without needing to be replaced or recharged. Studies have been focused in linear and nonlinear energy harvesting devices^{1, 2, 3, 4, 5, 6, 7}. The main disadvantage of the linear energy harvesting device is that it produces the most power only at the resonance frequencies. Because the range of ambient vibrations is broad, nonlinear energy harvesting has been explored and studied. The idea of nonlinear energy harvesting is that a particular device can have a broad range of resonance frequencies in which there is an optimal generation of power¹⁶. A variety of nonlinear harvesting devices and mechanisms have been proposed in the recent years, all having their own advantages and disadvantages. Several types of devices were discussed in the recent review articles: including the inverted pendulum with polar opposing magnets, the bi-stable plate with piezoelectric elements, and the dual-clamped post-buckled beam^{14, 15, 16, 19}. These studies compare these devices to each other and describe their effectiveness against linear energy harvesting devices. A device proposed by Cottone et al. (2009) included an inverted pendulum and a set of magnets, one fixed to the end of the pendulum and one fixed to a stand¹⁶. The pendulum was excited at the base to generate oscillations at the tip. The magnets would cause the tip to oscillate violently and, using a resistive circuit, generate a voltage across a load resistor. The distance between the magnets was optimized so that there would be two stable locations for the pendulum when no oscillations were induced. The oscillations would cause the pendulum to jump between the two stable states and generate chaotic oscillations, where a large amount energy could be harvested. Stanton et al. (2010) improved on the idea and proposed an inverted pendulum using a piezoelectric beam composite as its basis¹⁷. Their idea was to be able to tune the device using a specialized circuit to achieve an enhanced response at a given ambient excitation. However, these types of devices were heavier to implement. They concluded that small electrical perturbations could induce the device to achieve better vibrational responses to a given input. Arrieta et al. (2010) proposed a piezoelectric bi-stable plate to harvest vibrational energy⁵. This configuration included a square laminate with piezoelectric elements held by an electromechanical shaker at the center. The laminate was manufactured with two stable states to allow for snap-through dynamics during chaotic oscillations^{10, 11}. They concluded that chaotic oscillations generated a significant amount voltage in the piezoelectric elements and that the device did not need external weights to

aid in inducing chaotic oscillations. Arrieta et al. (2013) then combined the inverted pendulum and bi-stable laminate into a cantilevered bi-stable beam⁴. This configuration performed better than the post-buckled beam when measuring the voltages near the clamp root. This method was improved by Scarselli et al. (2016) by modifying the clamp and pin locations of the beam to reduce the required excitation force and increase energy harvesting potential¹⁸. The beam would be clamped at one end and simply supported at a certain distance from the clamp. Similar frequency response optimizations and observations were made. Throughout all of the previous mentioned devices and experiments it was discovered that a range of resonance frequencies could produce chaotic oscillations on the device and generate more average power than a linear oscillator. Designing efficient energy harvesting circuits or optimizing the laminate dimensions and composite can improve the energy harvesting capabilities of the device. These laminates can also be used for other applications such as morphing structures or structures with variable stiffness¹⁹. The goal of this project is to investigate the behavior and response of a clamped-clamped bi-stable element to better prepare the designs and predict the performance of future energy harvesting devices.

2. CONCEPT

2.1 Clamped-clamped multi-stable laminate

Composite materials with sections of various fiber orientations can create multiple equilibrium states as a result of thermal strain and expansion¹⁹. Alternating between these equilibrium states is also possible via snap-through after applying a certain amount of activation energy. The laminate considered in this paper has seven sections of various carbon fiber orientation profiles which are cured together at 140°C, then cooled and relaxed at room temperature. Once cooled, the laminate deforms due to thermal strain and stabilizes as shown in Figure 1¹³. The final dimensions of the laminate are 212 mm length and 64 mm width. The laminate is then clamped at the ends and buckled as shown in Figure 2 to a final length of 190mm. Now, there are two different stable configurations of the laminate, one at either side of the buckle. Adding additional mass to the laminate at locations that have the most curvature, near the clamp in this case, would allow the laminate to snap more easily from one state to the other. This would allow for a more visible snap-through motion at higher excitations. The weight of the magnets used for low amplitude resonance is 8 grams. The weight of the larger magnets to be used for the snap-through experiments are 44.8 grams. Figure 3 shows the energy of the system compared to the displacement. It can be observed that the well at state 2 has a higher energy state than at state 1.

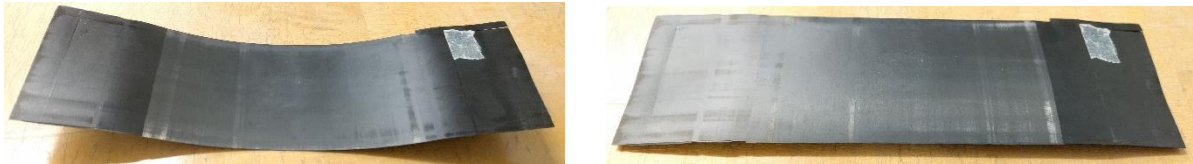


Figure 1. (a) Cured laminate at state 1 (low). (b) Laminate at state 2 (high).



Figure 2. (a) Clamped-clamped laminate positioned at state 1 (low) with mass on the sides to aid in inducing larger oscillations. (b) Laminate positioned at state 2 (high).

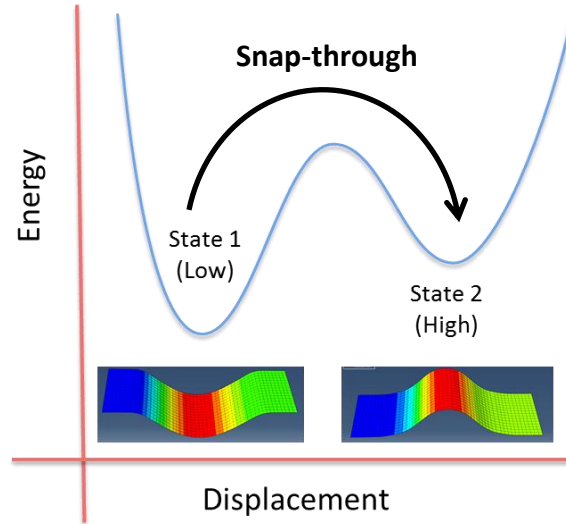


Figure 3. Energy vs. displacement plot^{8,9}. State 1 has a low energy well and state 2 has a high energy well. Below each well is a finite element model of the respective stable states.

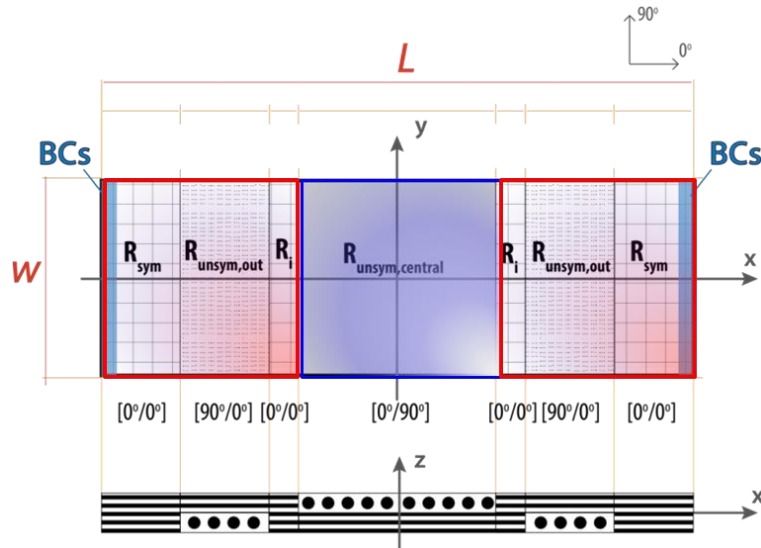


Figure 4. Fiber orientations along the laminate. There are 7 sections that, when thermally cured, generate bi-stable properties⁸.

2.2 Inter-well oscillations

During resonance, the laminate exhibits an increased amplitude response. It is predicted that certain responses can be large enough to cause a snap-through to the next stable state. Recurring snap-through motion between these states is known as inter-well oscillations. This type of motion is projected to have chaotic responses and is able to generate large strains near the clamp root¹². For harvesting energy, the inter-well oscillations are to be exploited by resonating the laminate and transforming the strains near the clamp into a voltage via embedded piezoelectric elements. During snap-through motion, the strain near the clamps vary greatly with respect to the rest of the laminate. This is where the piezoelectric material would be placed to optimize the energy harvesting potential.

3. FINITE ELEMENT MODEL

3.1 Modelling

The laminate is modelled in Abaqus CAE to simulate the thermal curing process and determine the modal frequencies and shapes for various configurations. The carbon fiber section orientation for the laminate is shown in Figure 5. Point masses with the mass and moment of inertia properties of the magnets used during the experiments are placed at the center, $(X, Y, Z) = (0, 0, 0)$ mm, or at the sides, $(X, Y, Z) = (\pm 59, 0, 0)$ mm. The model is calculated using a standard static analysis considering nonlinear geometry. First, the laminate is heated to 140°C , then cooled to 0°C while being relaxed to simulate the curing process undergone by the laminate during manufacturing. Then, the ends of the laminate are constrained horizontally as the right edge moves towards the left at a determined value. This simulates the clamping effect that represents state 1 of the specimen, as shown in Figure 6. To clamp to state 2, a displacement step is added before the clamping step so that the center of the laminate is above the XY-plane. Several mass and clamp configurations are studied and simulated to better predict the behavior of the laminate during vibrational responses. To determine the modal properties at state 1 and 2, a perturbation step is conducted after the clamping step to calculate the first ten resonant frequencies and shapes.

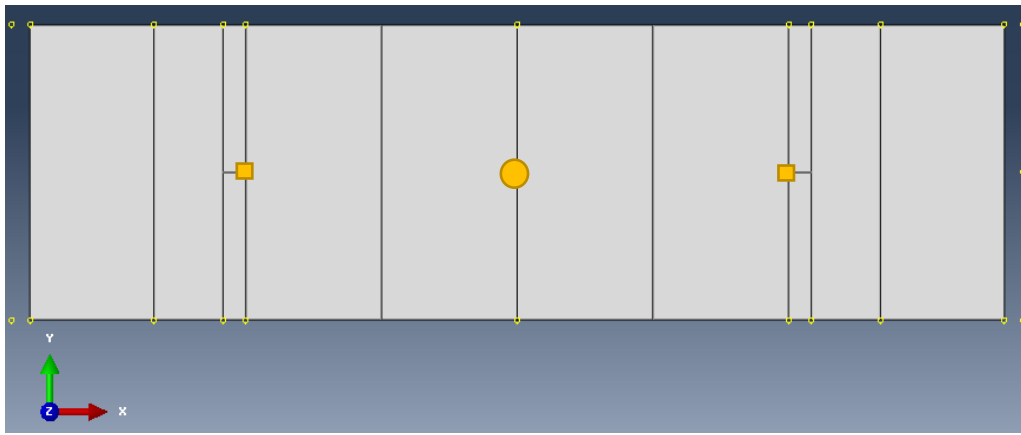


Figure 5. Section Configuration of the laminate in Abaqus CAE. The point mass locations are either at the center, at the yellow circle, or at the sides, at the yellow squares.

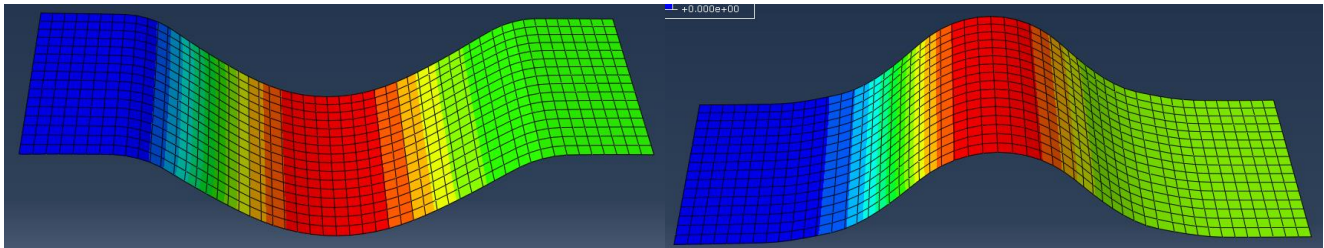


Figure 6. (a) Simulated clamp at state 1. (b) Simulated clamp at state 2 after applying displacement boundary condition.

3.2 Modal analysis and mass configuration

Table 1 displays the simulation properties with various mass configurations, including no mass, and the first six calculated modal frequencies for each stable state. The masses are assumed to be in the form of a disk or cuboid to represent the physical magnet masses used in the experiments. The modal frequencies tend to decrease with increased mass, as expected. The placement of the mass has complex effects with the characteristics of the modal frequencies and shapes. For the simulations with mass at the center, the modal frequencies tend to group together at certain ranges. As for the modal shapes, some of the deformation modes resemble twists and complex displacements along the Y-direction. These have very little deformations near the clamp root, where the piezoelectric elements would be placed to generate a voltage. Because the piezoelectric device works best when there is a large change in curvature²⁰, this type of shape provides little

capability for energy harvesting. There are also shapes that resemble symmetric and asymmetric out of plane deformations along the X-direction, showing large displacements near the clamp root. This is particularly desired for optimal energy harvesting because of the large changes in curvature. Figures 7, 8, and 9 show the scaled modal shapes for the various configurations. The modal shapes and frequencies are similar between state 1 and state 2, showing the tendency of the laminate to maintain a similar shape during inter-well oscillations. Compared to the simulation without any mass, the resonant frequencies are much closer together. This could improve broadband energy harvesting by allowing the laminate to be held in resonance consistently for that particular range. For the simulations with two masses at the sides, the resonant frequencies are similarly close together for a small range but slightly more spread out. The modal shapes at these configurations are more similar to the symmetric and asymmetric bend patterns, and there are less complex twist patterns. This shows that there is more capability for energy harvesting in the configurations that include equal masses at the sides. Again, similar shapes were observed at state 1 and state 2, however these occur at slightly different frequencies. Modifying the clamp length parameter was also considered in the study, however it seems it has very little effect on the modal properties. Large changes in the clamp length are not considered because of the limitations of the apparatus, however small changes were considered and simulated. Results show that the resonant frequencies generally tend to increase as the clamp length increases and vice versa. The modal shapes are very similar to the original simulations and still include the same amount of shape variation for each mass configuration.

Table 1. Simulation properties for various mass configurations. The clamp length was held constant for these simulations. The masses were assumed to be either disks or cuboids to represent the physical magnets used during the experiments. The first six modal frequencies are presented for each stable state, state 1 (low) and state 2 (high).

Mass Configuration	Mass locations (mm)	Mass amount (grams)	Mass moment (x,y,z) (grams × mm ²)	Modal Frequencies (Hz) State 1 (L) State 2 (H)
No Mass	-	-	-	91.097, 111.26, 156.11, 182.78, 303.6, 320.56
				69.015, 71.284, 101.71, 163.23, 232.95, 385.01
1 Mass at the Center (Disk)	(0, 0, 0)	22.6	(1562.91666, 1562.91666, 1512.5)	29.762, 36.281, 36.9, 56.113, 63.665, 71.162
				23.129, 26.747, 36.515, 41.873, 46.71, 74.155
1 Small Mass at the Center (Disk)	(0, 0, 0)	11.3	(195.365, 195.365, 189.062)	60.773, 72.757, 99.018, 99.052, 107.56, 108.2
				31.962, 56.948, 61.28, 97.553, 102.78, 114.86
1 Large Mass at the Center (Disk)	(0, 0, 0)	45.2	(6251.68, 6251.68, 3025)	15.304, 18.572, 25.671, 40.606, 47.581, 50.755
				13.722, 15.533, 22.692, 25.826, 34.559, 55.117
2 Masses at the Sides (Cuboid)	(-59, 0, 0) (59, 0, 0)	6 × 2	(162.5, 62.5, 125)	55.748, 77.815, 94.401, 110.57, 131.79, 146.82
				40.741, 54.091, 65.933, 119.51, 134.33, 157.75
2 Small Masses at the Sides (Cuboid)	(-59, 0, 0) (59, 0, 0)	4 × 2	(66.6667, 41.6667, 41.6667)	63.225, 91.716, 106.43, 139.52, 183.88, 188.33
				46.246, 62.153, 69.238, 161.96, 169.75, 183.76
2 Large Masses at the Sides (Disk)	(-59, 0, 0) (59, 0, 0)	22.6 × 2	(1562.91666, 1562.91666, 1512.5)	28.083, 33.204, 35.606, 38.406, 42.949, 50.915
				21.458, 27.723, 32.799, 38.654, 45.041, 47.192

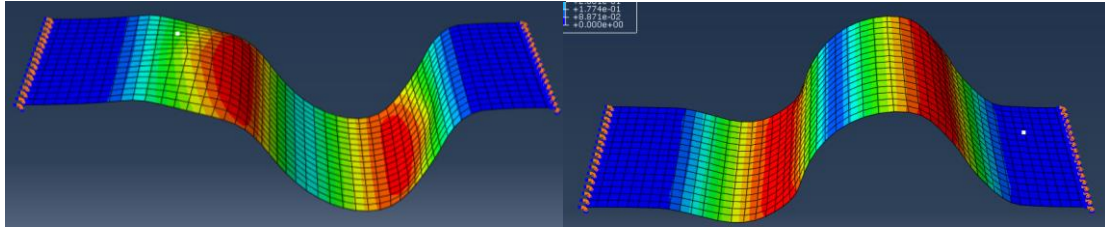


Figure 7. Scaled modal shapes at state 1 and state 2 respectively. These shapes show the asymmetric wave pattern that is more common in the configuration with two masses on the sides of the laminate and occur at the lower end of the calculated resonant frequencies. It is shown that the most deflection from the xy-plane occurs near the clamp root, where the piezoelectric elements would be placed to convert strain into electricity.

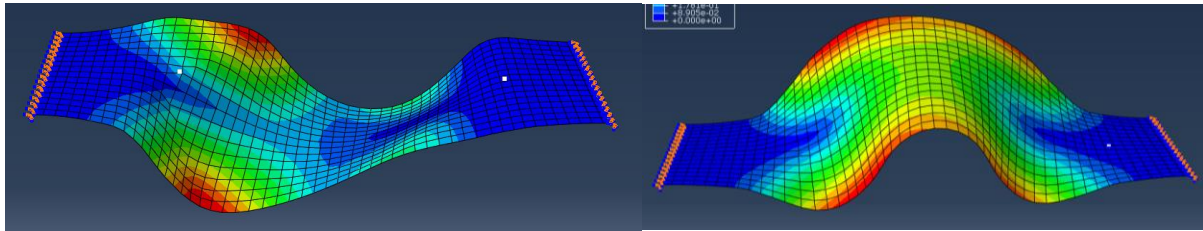


Figure 8. Scaled modal shapes at state 1 and state 2 respectively. These shapes represent the complex twisting resonant motions that occur mostly in the configurations that involve one mass at the center of the laminate. These motions do not show significant displacement or strain near the clamp root, therefore these shapes do not show significant capability for energy harvesting.

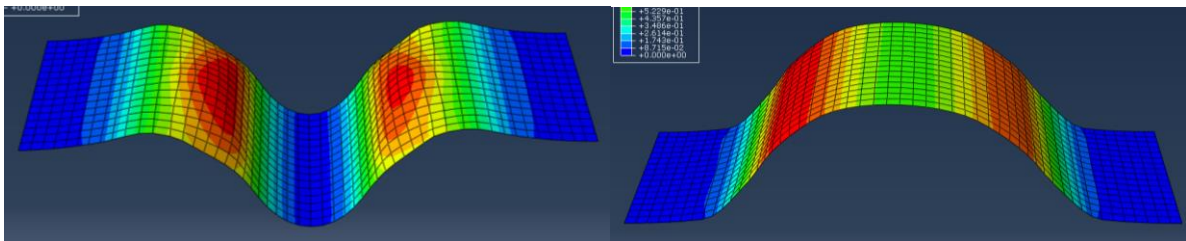


Figure 9. Scaled symmetric modal shapes at state 1 and state 2 respectively. These shapes occur mostly in configurations with two masses at the sides of the laminate and occur at a higher resonant frequency. These shapes show significant displacement near the clamp root.

4. EXPERIMENTAL RESPONSE

4.1 Apparatus and procedure

The experiments are conducted with a large electromechanical shaker and a base plate with the laminate clamped in place. The magnet masses are located in the various configurations as simulated earlier. The base plate and laminate rig is shown in Figure 10. Two displacement lasers are placed above the laminate, one aimed at the top of the clamp head on the rig and one 20 mm from the clamp on the laminate. Figure 11 shows the schematic of the apparatus and data acquisition setup that is used in the experiments. An accelerometer is placed at the center of the base plate of the shaker to record the input signal to verify the excitation level. Another accelerometer is placed at the same location for the feedback to the shaker controller. Due to the practical limitations of the apparatus and the shaker, the minimum possible level of input excitation could not fall below 1g of acceleration and 10Hz. The upper limit did not exceed 7g and 100Hz to prevent damage to the apparatus and laminate and to avoid internal resonance within the cooling system of the shaker. To measure a linear response, the laminate is excited at a sinusoidal input while sweeping from 10Hz to 100 Hz at 1Hz/s. Then, the sweep range is reduced to values near the previously observed resonant regions and the sweep rate is reduced to 0.1Hz/s or

0.2Hz/s. This greatly reduces the possibility of recording significant continuous transience and aids in maintaining a linear response. For significantly nonlinear responses, a step-sine sweep is used to alleviate the effects of transience during the test. The various mass configurations are tested to compare the empirical response with the simulated data. Observations are made noting the shape and behavior of the laminate during certain resonance periods for the various tests. This procedure is repeated for both stable states. Once the linear response is recorded, the amplitude of the shaker is increased to study the ability of the laminate to snap-through and between the stable states. The procedure is again repeated for the various mass configurations and stable states.

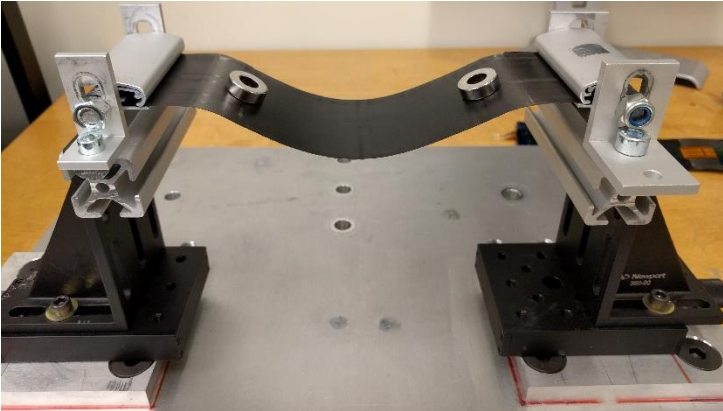


Figure 10. Laminate clamped onto baseplate rig. This rig is fixed to the TIRA shaker.

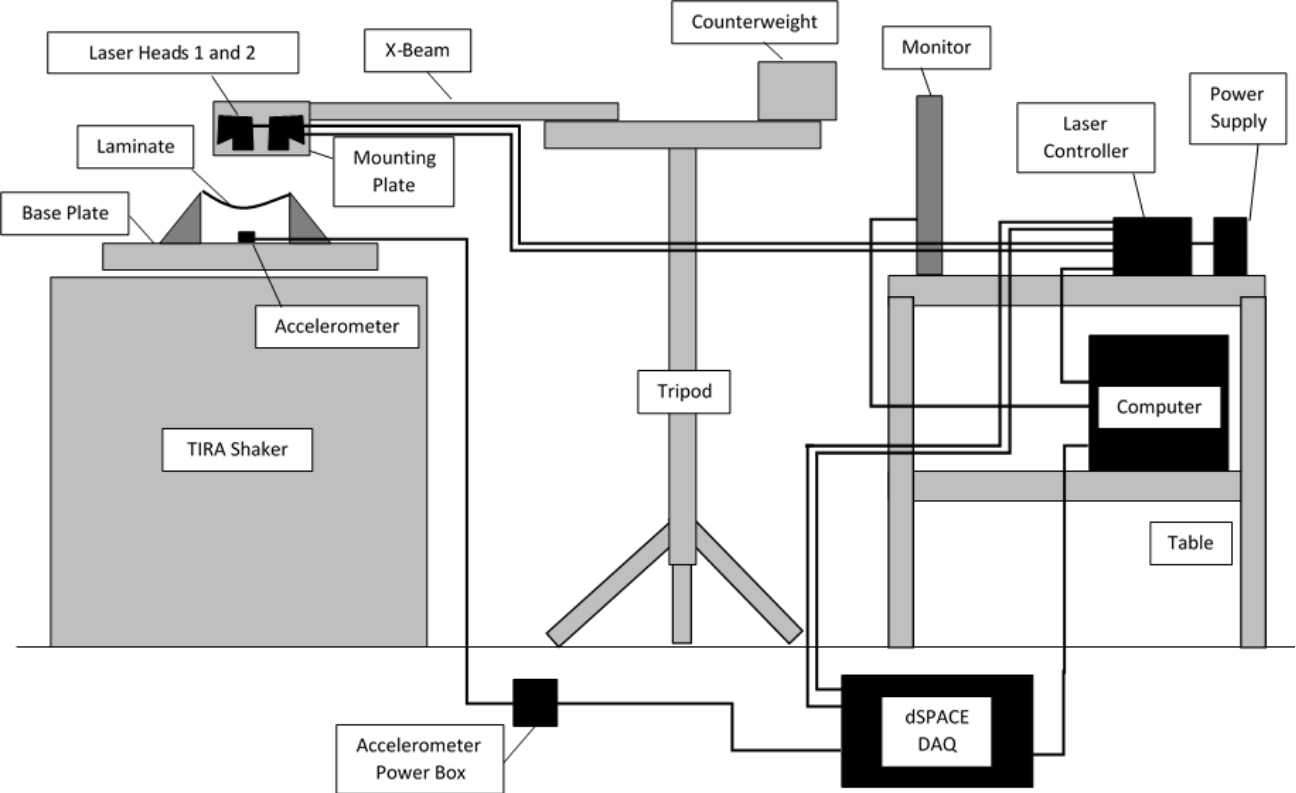


Figure 11. Schematic of the experimental apparatus. The laser heads can measure to an accuracy of $\pm 0.001\text{mm}$. The data was sampled and recorded at $10,000\text{Hz}$.

4.2 Modal properties about the stable states

Table 2 lists the resonant frequencies observed from each of the experimental trials along with the testing parameters. The observed resonant frequencies are not very similar to the simulated results obtained from the finite element analysis, however they fall within a similar range as the simulated results. This is likely due to the simplification of the point mass in the model and the imperfections in the laminate. Although the resonant frequencies differ, the observed shapes match the expected outcome. There are more twisting motions with laminates that have the mass at the center. There are also asymmetric and symmetric wave-like patterns that can be seen for both mass configurations but more often for the configuration with the mass at the sides. It is found that small clamp length variations have little effect on the location of the resonant frequencies and modal shapes, however as the length increases, the required force to snap between the stable states tends to decrease. Figures 12 and 13 shows the linear response and the frequency response of the laminate at state 1 (low) for the two-mass configuration at the sides at a 1g excitation. A closer inspection at the response indicates that the oscillations are purely sinusoidal and linear. Here, the resonant locations can be seen at around 33Hz and 41Hz. The reason behind the increased displacement at around 110s is due to the modal shape of the laminate at that frequency. This shape is similar to the symmetric wave shape shown in Figure 9 and therefore causes the increase in displacement. These resonant frequencies are verified by the Fast Fourier Transform shown in Figure 13. A similar linear response is observed for state 1 as well. During the frequency sweeps, the laminate resonates at lower frequencies and has increased displacement amplitudes when decreasing the input frequency. This shows the nonlinear behavior of the device as the frequency changes. Transience tends to last for several seconds more for the center mass configuration than for the side mass configuration.

Table 2. Observed resonant frequencies from empirical results. The testing parameters are also listed for various mass configurations and excitation levels.

Mass locations (mm)	Mass amount (grams)	Excitation Level (g)	Observed Resonance Frequencies (Hz) State 1 (L) State 2 (H)
(0, 0, 0)	17.5	1g	44.57
			24.95, 59.49
(0, 0, 0)	22.6	1.5g	45, 76
			19, 26, 48, 60
(0, 0, 0)	45.2	1g	13, 22, 36, 43
			24, 38, 43
(-59, 0, 0) (59, 0, 0)	22.6 × 2	1g	22, 27
			24
(-59, 0, 0) (59, 0, 0)	6 × 2	1g	-
			26.74, 33.29
(-59, 0, 0) (59, 0, 0)	4 × 2	1g	53.72
			33.09, 41.13

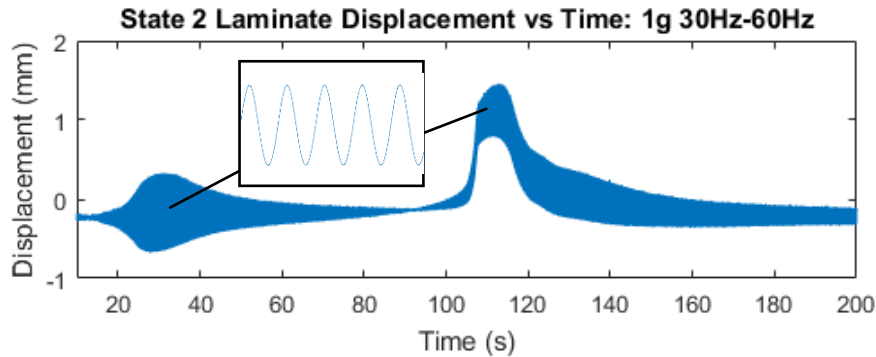


Figure 12. Displacement vs time graph for the laminate at state 2 with two 4 gram masses at the sides. The increased displacement at 110s is due to the modal shape of the laminate at that particular frequency.

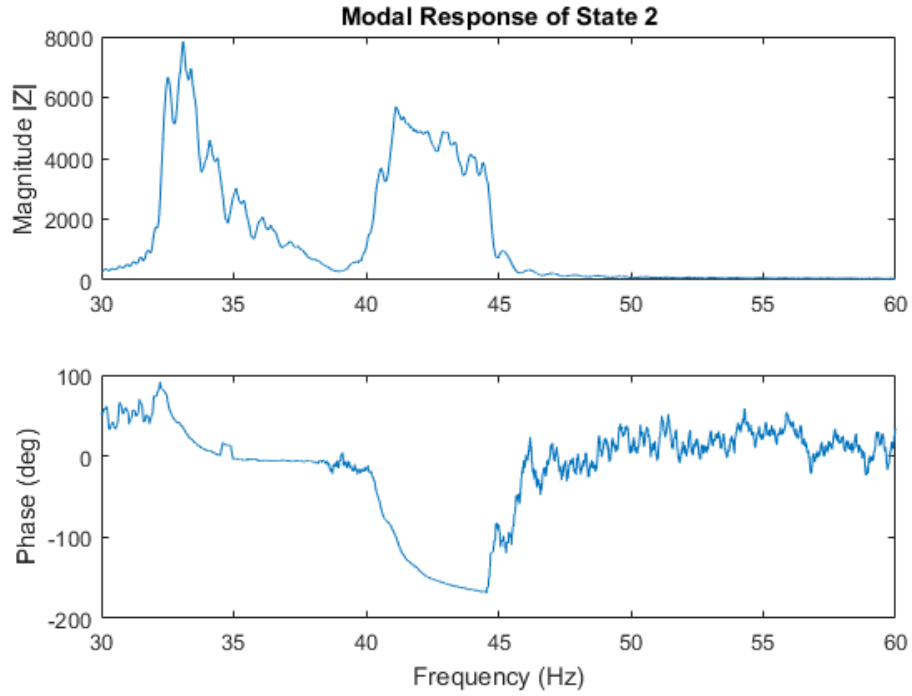


Figure 13. Frequency response function of response from Figure 12. The peaks represent the magnitude of the vibrational response. The resonant frequencies are observed at these peaks and when there is a 90 degree phase shift. This function is used to calculate the resonant frequencies of the laminate for the given input.

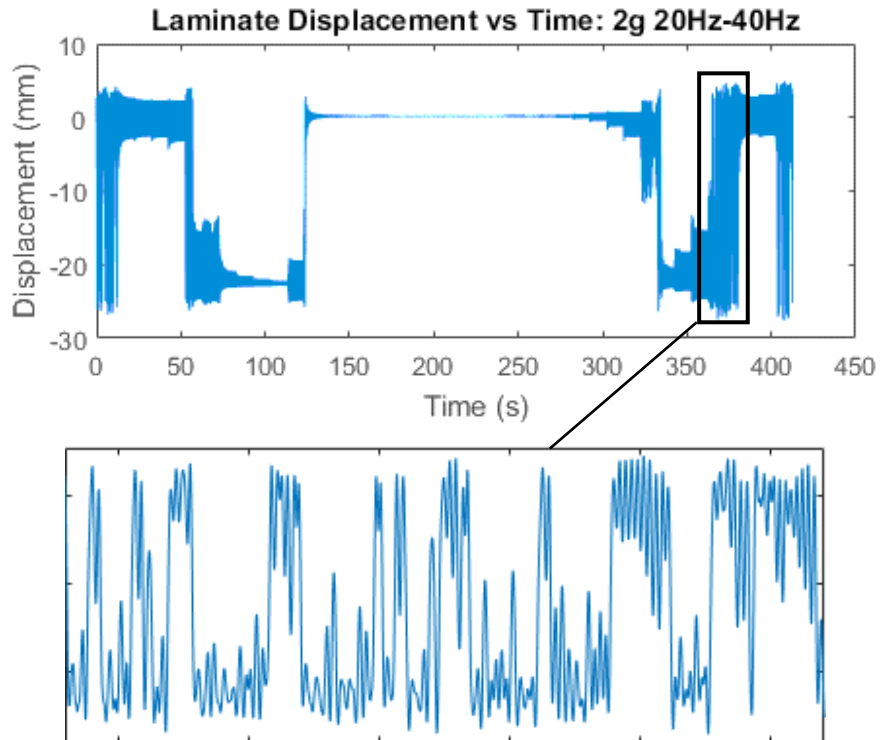


Figure 14. The graph on top is the time response of laminate under a higher excitation level. Here, 0 mm represents state 1 and -20 mm represents state 2. The graph below shows a smaller time period in which there are continuous oscillations between both states. This time frame occurs at a frequency around 24Hz.

4.3 Snap-through response: inter-well dynamics

To induce snap-through dynamics, the laminate is excited at larger amplitudes while maintaining the same frequency ranges and sweep rates. Figure 14 shows the time response of the laminate for a mass configuration with two 22.6g masses at the sides. A closer look at a time period in which inter-well oscillations are present shows a chaotic motion between the two states. This is especially useful for energy harvesting as chaotic motion between the states indicates large deformations near the clamp, which has been shown to generate more average power when a piezoelectric element is embedded to the laminate at that location^{14, 15, 18}. It can also be noted from the time response data that the laminate can snap between the stable states at certain frequencies fairly consistently.

5. CONCLUSIONS

The linear and nonlinear oscillations of a clamped-clamped multi-stable laminate has been experimentally studied in this paper. The finite element method is used to examine the modal frequencies and shapes about each of the stable states. Large amplitude oscillations and complex dynamics are observed when excited at various amplitudes and frequencies for numerous mass configurations. The modal shapes have an effect on the overall displacement of the laminate and can be controlled by mass placement. If the mass is placed at the center, the laminate experiences more twisting motion during resonance and the resonant frequencies tend to be immediately adjacent to each other. If the mass is placed at the sides near the clamps, the modal shapes are more like planar bends that can be asymmetric or symmetric along the X-direction. These types of mode shapes seem to show the most capability for snap-through motion and thus energy harvesting. Studies need to be performed in understanding how mass placement affects modal frequency placement and shape deformation. Future projects would include placing piezoelectric elements onto the laminate and verify the capability of the device to harvest energy from various input excitations. The previous procedure would be repeated with this piezoelectric embedded laminate along with the various mass configurations. Another project would include placing the device in an array of bi-stable elements for mechanical diodes to study the energy harvesting capabilities presented^{8, 9}. Mathematical modelling would also need to be conducted to provide a better understanding of the complex behaviors presented in this paper. More work would be done in refining the finite element model and calculations so that a relation can be seen between the empirical and simulated results. The experimental data can be improved by using camera system to record the displacement for the entire area of the laminate during the excitations.

6. ACKNOWLEDGEMENTS

We would like to thank the Summer Undergraduate Research Fellowship (SURF) Program at Purdue for funding and supporting the research. Herrick Laboratories is home to the Smart Materials and Adaptive Structures Lab (SMASL) at Purdue University. We would also like to thank Jelena Parapovic, Allison Range, and Dr. Jeff Rhoads for aiding us in using the TIRA shaker for our experiments.

REFERENCES

- [1] A. F. Arrieta, O. Bilgen, M. I. Friswell and P. Hagedorn, "Dynamic control for morphing of bi-stable composites," *Journal of Intelligent Material Systems and Structures*, vol. 24, no. 3, pp. 266-273, 2012.
- [2] A. F. Arrieta, I. K. Kuder, M. Rist, T. Waeber and P. Ermanni, "Passive load alleviation aerofoil concept with variable stiffness multi-stable composites," *Composite Structures*, vol. 116, pp. 235-242, 2014.
- [3] I. K. Kuder, A. F. Arrieta, M. Rist and P. Ermanni, "Static design of a selective compliance morphing wing profile based on integrated variable stiffness bi-stable components," in *ASME 2014 Conference on Smart Structures, Adaptive Structures and Intelligent Systems (SMASIS2014), September 8-10, Newport, Rhode Island, USA*, 2014.
- [4] A. F. Arrieta, T. Delpero, A. E. Bergamini and P. Ermanni, "Broadband energy harvesting with cantilevered bi-stable composites," *Applied Physics Letters*, vol. 102, no. 17, p. 173904, 2013.
- [5] A. F. Arrieta, P. Hagedorn, A. Erturk and D. J. Inman, "A piezoelectric bi-stable plate for nonlinear broadband energy harvesting," *Applied Physics Letters*, vol. 97, no. 10, p. 104102, 2010.
- [6] D. N. Betts, H. A. Kim, C. R. Bowen and D. J. Inman, "Optimal configurations of bistable piezo-composites for energy harvesting," *Applied Physics Letters*, vol. 100, p. 114104, 2012.

- [7] D. N. Betts, C. R. Bowen, H. A. Kim, N. Gathercole, C. T. Clarke and D. J. Inman, "Investigation of bistable piezo-composite plates for broadband energy harvesting," in *Proceedings of the SPIE. Active and Passive Smart Structures and Integrated Systems*, 2013.
- [8] N. Nadkarni, A. F. Arrieta, C. Chong, D. M. Kochman and C. Daraio, "Unidirectional Transition Waves in Bistable Lattices," *Physical Review Letters*, vol. Under review, 2016.
- [9] N. Nadkarni, C. Daraio and D. M. Kochmann, "Dynamics of periodic mechanical structures containing bistable elastic elements: From elastic to solitary wave propagation," *Physical Review E*, vol. 90, p. 023204, 2014.
- [10] A. F. Arrieta, O. Bilgen, M. I. Friswell and P. Hagedorn, "Passive load alleviation bi-stable morphing concept," *AIP Advances*, vol. 2, no. 3, p. 032118, 2012.
- [11] A. F. Arrieta, I. K. Kuder, T. Waeber and P. Ermanni, "Embeddable Variable Stiffness Multi-stable Composites," in *24th International Conference on Adaptive Structures and Technologies (ICAST), Aruba, October 7-9, 2013*.
- [12] A. F. Arrieta, S. A. Neild and D. J. Wagg, "On the cross-well dynamics of a bi-stable composite plate," *Journal of Sound and Vibration*, vol. 330, no. 14, pp. 3424-3441, 2011.
- [13] K. D. Murphy, L. N. Virgin and S. A. Rizzi, "Experimental snap-through boundaries for acoustically excited, thermally buckled plates," *Experimental Mechanics*, vol. 36, pp. 312-317, 1996.
- [14] Pellegrini, S. P., Tolou, N., Schenk, M. and Herder, J. L., "Bistable vibration energy harvesters: A review," *Journal of Intelligent Material Systems and Structures*. May 28, 2012.
- [15] Harne, R. L., and Wang, K. W., "A review of the recent research on vibration energy harvesting via bistable systems". *Smart Materials and Structures* Vol. 22, No. 023001. Jan. 25, 2013.
- [16] Cottone, F., Vocca, H., and Gammaitoni, L., "Nonlinear Energy Harvesting". *Physical Review Letters* Vol. 102, No. 080601. Feb. 23, 2009.
- [17] Stanton, S. C., McGehee, C. C., and Mann, B. P., "Nonlinear dynamics for broadband energy harvesting: Investigation of a bistable piezoelectric inertial generator". *Elsevier: Physica D* Vol. 239, p. 640-653. Feb. 1, 2010.
- [18] Scarselli, G., Nicassio, F., Pinto, F., Ciampa, F., Iervolino, O., and Meo, M., "A novel bistable energy harvesting concept," *Smart Materials and Structures* Vol. 25, No. 055001. Mar. 30, 2016.
- [19] Emam, S. A., and Inman, D. J., "A Review on Bistable Composite Laminates for Morphing and Energy Harvesting," *Applied Mechanics Reviews*. Vol. 67, No. 060803. Nov 2015.
- [20] Leo, D., *Engineering Analysis of Smart Material Systems*. John Wiley & Sons, Inc., 2007: p. 122-176